Role of bulk-magnon transport in the temporal evolution of the longitudinal spin-Seebeck effect

M. Agrawal,[1,2,*] V. I. Vasyuchka,[1] A. A. Serga,[1] A. Kirihara,[1,3] P. Pirro,[1] T. Langner,[1] M. B. Jungfleisch,[1] A. V. Chumak,[1] E. Th. Papaioannou,[1] and B. Hillebrands[1]

[1]*Fachbereich Physik and Landesforschungszentrum OPTIMAS, Technische Universität Kaiserslautern, 67663 Kaiserslautern, Germany*
[2]*Graduate School Materials Science in Mainz, Gottlieb-Daimler-Strasse 47, 67663 Kaiserslautern, Germany*
[3]*Smart Energy Research Laboratories, NEC Corporation, Tsukuba 305-8501, Japan*

We present the temporal evolution of the longitudinal spin Seebeck effect in a YIG|Pt bilayer system. Our findings reveal that this effect is a submicrosecond fast phenomenon governed by the thermal-magnon diffusion along the thermal gradient inside the magnetic material. A comparison of experimental results with the thermal-driven magnon-diffusion model demonstrates that the temporal behavior of this effect depends on the time development of the temperature gradient in the magnetic material close to the interface. The effective thermal-magnon diffusion length for the YIG|Pt system is estimated to be around 500 nm.

The spin Seebeck effect (SSE) [1–7] is one of the most fascinating phenomena in the contemporary era of spin-caloritronics [8]. Analogous to the classical Seebeck effect, the SSE is a phenomenon where a spin current is generated in spin-polarized materials like metals [2], semiconductors [4,5], and insulators [6,7] on the application of a thermal gradient. Generally, the generated spin current is measured by the inverse spin Hall effect (ISHE) [9] in a normal (diamagnetic, paramagnetic) metal like Pt, placed in contact with the magnetic material. Currently, this phenomenon has attracted much attention due to its potential applications. For example, recent progresses show that based on this effect thin-film structures can be fabricated to generate electricity from waste-heat sources [10]. Further advancements in industrial applications like temperature sensors, temperature gradient sensors, thermal spin-current generators, etc., require an in-depth understanding of this effect.

Although there have been numerous experimental and theoretical studies about this effect, the underlying physics remains unsettled. The most accepted theory predicts that the SSE is driven by the difference in temperatures of magnon, phonon, and electron baths of the system [11,12]. However, no clear evidence of such difference has been observed experimentally when an in-plane thermal gradient is applied to the magnetic material [13]. Some studies show that the interface proximity effect in the YIG|Pt system, which is responsible for partial magnetic polarization of the Pt layer, could lead to similar behavior due to the anomalous Nernst effect as observed for the SSE [14]. However, very recent measurements claim no visible contribution of the proximity effect to the SSE voltage [15–17]. Another ambiguity is whether the SSE is a pure interface effect or the vicinity of the interface plays a significant role (bulk contribution) [18,19].

To shed light on the controversial physics, we developed an entirely new experimental approach where we studied the temporal evolution of the SSE in YIG|Pt bilayer structures. The observations were realized in the longitudinal configuration of the SSE [7]. In the longitudinal spin Seebeck effect (LSSE), a thermal gradient is applied perpendicular to the film plane

which generates a spin current along the thermal gradient. From our measurements, we find that a certain volume of the YIG film in the vicinity of the interface effectively contributes to the LSSE, and the temporal dynamics of the LSSE voltage strongly depends on the magnon transport in this YIG volume.

The LSSE measurements were performed on a bilayer of a magnetic insulator, yttrium iron garnet (YIG), and a normal metal, platinum (Pt). A 6.7-μm-thick YIG sample of dimensions 14 mm × 3 mm was grown by liquid phase epitaxy on a 500-μm-thick gallium gadolinium garnet (GGG) substrate. To achieve a good YIG|Pt interface quality, a detailed YIG surface cleaning process [20] was followed. A strip (3 mm × 100 μm) of 10-nm-thick Pt was deposited on the cleaned YIG surface, by molecular beam epitaxy at a pressure of 5×10^{-11} mbar with a growth rate of 0.05 Å/s. In Fig. 1, a schematic diagram of the experimental setup is shown. Unlike electric heating techniques, where spurious induction voltage interferes with the relatively small LSSE voltage, a laser heating technique [21–23] was employed to heat the Pt strip from the top surface in order to create a vertical thermal
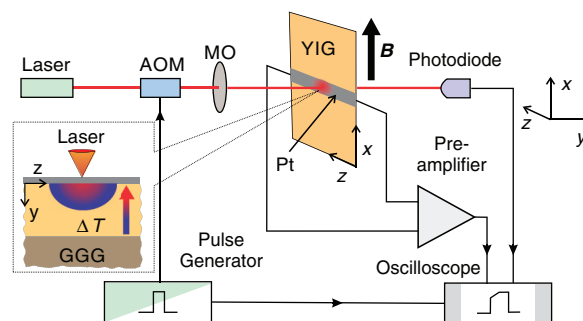

FIG. 1. (Color online) Sketch of the experimental setup. A continuous laser beam (wavelength 655 nm), modulated by an acousto-optical modulator (AOM), was focused down on a 10-nm-thick Pt strip, deposited on a 6.7-μm-thick YIG film, by a microscope objective (MO). The laser intensity profile was monitored by an ultrafast photodiode. An in-plane magnetic field $B = 20$ mT was applied to the YIG film. The heated Pt strip created a thermal gradient perpendicular to the YIG|Pt interface (see the inset). The generated voltage across the Pt strip due to the ISHE was amplified and measured by an oscilloscope.
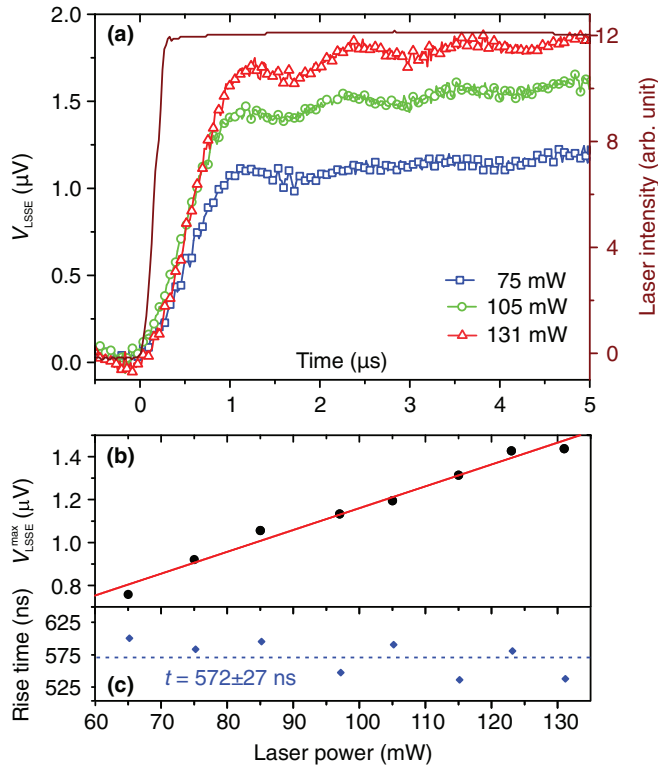
*magrawal@physik.uni-kl.de

FIG. 2. (Color online) (a) The time profiles of the laser intensity (solid line), and the LSSE voltage (V_{LSSE}) at various laser powers of 75 (square), 105 (circle), and 131 (triangle) mW. The oscillation in the signal is just an artifact due to the preamplifier observed even at zero level of the signal. (b) Measured V_{LSSE}^{max}, with linear fitting, and (c) the rise time t as a function of the laser power. The rise time is practically independent of the laser power.

gradient along the y direction perpendicular to the bilayer interface (see Fig. 1). For this purpose, a continuous laser beam (wavelength 655 nm) was modulated by an acousto-optical modulator (AOM), and focused at the middle of the Pt strip using a microscopic objective (Leitz PL 16x/0.30) down to a laser spot size of 20–70 μm. The temporal profile of the laser beam was monitored simultaneously by observing the transmitted laser light through the YIG sample using an ultrafast photodiode. A rise time (10%–90%) of 200 ns was observed for the laser pulses [solid line in Fig. 2(a)]. The sample structure was mounted on a copper block to provide a thermal heat sink.

The time-resolved measurements of LSSE were carried out using 10-μs-long laser pulses with a repetition rate of 10 kHz. The repetition rate was chosen such that the sample gets enough time to cool down between the two consecutive laser pulses. An in-plane magnetic field $B = 20$ mT was applied to saturate the YIG film magnetization along the x direction. As a result of the LSSE, a spin current flows along the y direction. Due to spin-dependent electron scattering, the spin current converts into an electric field along the z direction in Pt. The electric field was detected as a potential difference V_{LSSE} between the two short edges of the Pt strip (shown in Fig. 1). The LSSE voltage V_{LSSE} was amplified by a high input-impedance preamplifier and monitored on an oscilloscope. The measurements were performed for both

$\pm x$ directions of the magnetic field. The LSSE voltage inverts its polarity by reversing the direction of magnetic field [7]; an absolute average value of V_{LSSE} was evaluated to eliminate any thermal emf offset.

In Fig. 2(a), the temporal profile of the laser intensity and V_{LSSE} for different laser heating powers are plotted. The LSSE signal rises sharply for the first 1 μs and then gradually attains a saturation level V_{LSSE}^{max}. A rise time (10%–90%) of 572 ± 27 ns is observed for the LSSE signal. The rise time of the LSSE signal is different from the rise time of the laser intensity (≈ 200 ns), which provides a signature that the LSSE has no direct correlation with the laser intensity profile. Furthermore, the additional test experiments performed using microwave pulses with a rise time of ≈ 5 ns as a heating source give the identical rise time of the LSSE signal. With increasing laser power, V_{LSSE}^{max} increases linearly [Fig. 2(b)]. The linear tendency indicates that the laser heating is in the linear regime, and no nonlinear phenomena like rectification or negative deferential SSE [24] are involved in this process.

Our first hunch to interpret the rise time of the LSSE signal was to study the temperature evolution in the YIG|Pt system. Fortunately, the Pt strip grown over the YIG film can be utilized as an excellent resistance-temperature (RT) detector to measure the temperature at the surface of the YIG film. We performed the resistance measurements of the Pt strip to calculate the variation of the temperature in the YIG|Pt system by the laser heating. To do so, a constant current $I_c = 0.5$ mA was passed through the Pt strip (room temperature resistance $R_{Pt} \approx 508$ Ω), and the potential drop ($\Delta V_{Pt} = \Delta R_{Pt} I_c$) due to the heating of Pt was measured with the same experiment setup used for the V_{LSSE} measurements. In order to observe the saturation level, a much longer laser pulse of 4 ms was used to heat the Pt strip. In this case, the repetition rate was decreased to 2 Hz. Note that the thermal emf (few microvolts) has negligible influence on these measurements as the potential drop (ΔV_{Pt}) is very large (≈ 0.25 V). With the help of auxiliary measurements of static resistance versus temperature performed on the uniform heated Pt strip, we observe that the resistivity of the Pt strip scales linearly with the temperature. With a very simple analytical model, ΔV_{Pt} can be expressed in terms of temperature (T).

In Fig. 3, the variation in the average temperature of the Pt strip (ΔT, in arbitrary unit) is plotted for different laser powers. Note that the absolute value of ΔT at the laser spot
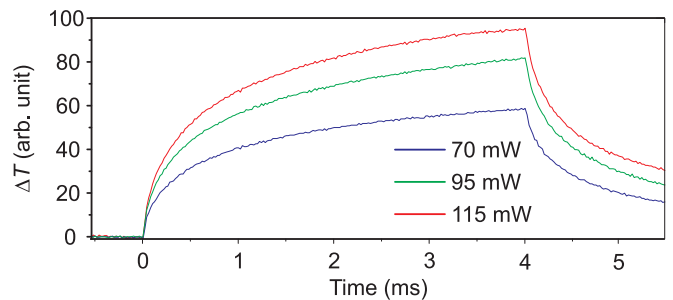

FIG. 3. (Color online) The time profile of the variation of temperature (ΔT) in the Pt strip on heating with a 4-ms-long laser pulse for various powers. Scale: 1 arb. unit ≈ 80–950 mK for the laser spot size 20–70 μm.

can not be calculated precisely due to a wide laser spot size (20–70 μm). A rise time of 2 ms was obtained for the average temperature of the Pt strip by fitting the data with a single saturating exponential function. The rise time is three orders of magnitude longer than the rise time of the LSSE signal [25]. Therefore, from the measurement of the Pt resistance, it can be concluded that the fast time scale of the LSSE cannot be described by the time scale of the variation in the average temperature of the system.

The next obvious hunch to interpret the rise times of the LSSE was the thermal gradient. The thermal gradient in the system was studied numerically by solving the 2D heat conduction equation for the YIG|Pt bilayer using the COMSOL Multiphysics simulation package [26]. The third dimension, i.e., the width of the Pt strip (100 μm) is neglected here for three reasons: (i) no (dc) ISHE voltage can be generated along this direction ($||\vec{B}$); (ii) the laser spot has a size comparable to the width of the Pt strip; and (iii) the COMSOL calculations show that no visible lateral broadening of the heated area occurs in the 2D geometry on the time scale (several microseconds) of the experiment.

In the simulation model, a stack of three rectangular layers, having lengths 300 μm each and thicknesses 10 nm (Pt), 6.7 μm (YIG), and 100 μm (GGG), was considered [see Fig. 4(a)]. The simulation parameters are indicated in Table I. The YIG|Pt interfacial thermal resistance [19] over a thickness of 5 nm was implemented in the simulations. As a boundary condition, the temperature along the bottom edge of the GGG layer was kept fixed at the room temperature (293.15 K). A 25-μm wide area at the middle of the Pt layer was considered as a heat source. The heat source, having lateral dimension (25 μm) larger than the YIG thickness (6.7 μm), replicates the laser heating spot in the experimental setup. In Fig. 4(b), the temperature distribution after 10 μs is presented. Since even after 10 μs, the temperature in the system changes only close to the heat source, the lateral dimension (300 μm) of the model geometry has no crucial impact on the study of the time scale of the LSSE.

In Fig. 4(c), the simulated temporal evolutions of the normalized variation in the average temperature (ΔT_{avg}) over the Pt strip and over the laser spot are shown. The average temperatures were evaluated by taking the average of temperatures along a line, parallel to the z axis at the middle of the Pt layer ($y = -5$ nm). The temporal evolution of ΔT_{avg} in the Pt strip was obtained (≈ 2 ms) as slow as it was observed in the Pt-resistance-measurement experiment. From simulations, we find that the gradual increase in the average temperature is due to the large heat capacity and volume of the system. The average temperature at the laser spot (heat source) varies visibly faster in comparison to the average temperature in the Pt strip but still significantly slower than the LSSE signal.

On the other hand, the thermal gradient close to the interface shows fast dynamics. We averaged the thermal gradient ∇T along lines parallel to the interface for various distances d from the interface in the YIG film [see Fig. 4(a)]. These parallel lines essentially represent the parallel planes (xz) in the experimental geometry. The average thermal gradient ∇T_{avg} at the interface was evaluated over a thickness of $\delta d = 5$ nm. In Fig. 4(d), the average thermal gradient for various distances d from the interface is shown. Contrary to the average temperature in Pt,

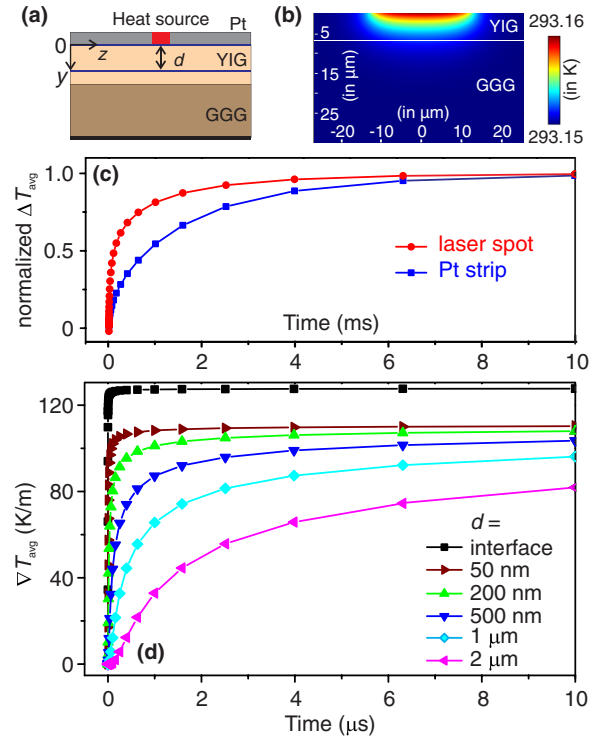FIG. 4. (Color online) (a) The 2D model geometry for the COMSOL simulations consisting three blocks (Pt, YIG, GGG) each of length 300 μm (along z axis) and thickness 10 nm (Pt), 6.7 μm (YIG), and 100 μm (GGG) along y axis. The thick horizontal line at the bottom represents the constant-temperature boundary (293.15 K). The heat source (25 μm) at the middle of the Pt layer replicates the laser spot. (b) The temperature distribution in YIG and GGG after 10 μs. Numerically calculated time profiles of (c) the normalized variation in the average temperature (ΔT_{avg}) over the Pt strip and the laser spot, and (d) thermal gradients ∇T_{avg} in YIG at the interface, and at $d = 50$ nm, 200 nm, 500 nm, 1 μm, and 2 μm distances away form the YIG|Pt interface.

the average thermal gradients rise very rapidly and saturate within microseconds. This time scale agrees with the time scale of the LSSE and gives a hint that the thermal gradient is a crucial quantity for the LSSE. As d, i.e., the depth of the reference line (a plane in a 3D model) from the interface, increases, the rise time of the temperature gradient raises due to the slow-down of the heat flow caused by the finite thermal conductivity and the increasing thermal capacity ($\propto$ volume).

TABLE I. Material parameters used for the numerical solution of the phonon heat transport equations in the YIG|Pt system.

Material	Density (kg/m^3)	Thermal conductivity (W/m K)	Heat capacity (J/kg K)
Pt	21450[a]	20[b]	130[a]
YIG	5170[d]	6.0[c]	570[e]
GGG	7080[c]	7.94[c]	400[c]

[a]Reference [27].
[b]Reference [28].
[c]Reference [29].
[d]Reference [30].
[e]Reference [31].

To explain the fast rising of the LSSE, we propose a phenomenological model—also supported by very recent theories [32,33]—where we consider the thermally-driven motion of magnons in a system of normal metal|magnetic material (e.g., Pt|YIG) subject to a thermal gradient perpendicular to the interface. In such a system, the spin current flowing in/out of the normal metal depends on the temperature difference of the magnon bath in the ferromagnet and the phonon bath (or electron bath) in the normal metal [11,12], and on the magnon accumulation close to the interface in the magnetic material. On the application of a temperature gradient, thermal magnons having higher population at hotter regions—in equilibrium their population is proportional to the phonon temperature—propagate towards colder regions having less magnon population. The propagation of magnons creates a magnon-density-gradient in the system along with the phonon-thermal-gradient. This implies that the spatial distribution of the magnon density depends on the magnon population (phonon temperature) and their propagation lengths. Therefore, the longitudinal spin Seebeck voltage can be considered as a combination of an interface effect and a bulk contribution from the magnon motions and, eventually, can be expressed as

$$V_{\text{LSSE}}(t) \propto \alpha \int_{-\delta d}^{0} \nabla T_y(y,t)\, dy$$
$$+ \beta \int_{0}^{l} \nabla T_y(y,t) \exp\left(\frac{-y}{L}\right) dy, \qquad (1)$$

where ∇T_y is the phonon thermal gradient perpendicular to the interface, l is the magnetic film thickness, and L is the effective magnon diffusion length. Here, δd represents the effective thickness of the interface. The parameter α defines the coupling between the electron bath in the normal metal and the phonon bath in the magnetic material. The coupling parameter β specifies the magnon-magnon interaction within the magnetic material. The phonon-magnon interaction is assumed to be sufficiently strong that no difference between the local phonon and magnon temperatures needs to be considered [13]. The first term of Eq. (1) includes the interface effects like proximity effect [14], interfacial thermal resistance [19], etc. Note that in this model, magnon diffusion times are neglected because the group velocity of magnons is much higher than that of phonons.

The fast rise of the thermal gradient ($\approx$20 ns) at the interface of the YIG|Pt bilayer, shown in Fig. 4(d), leads to the conclusion that the time scale of the LSSE cannot be explained by examining only the time evolution of the thermal gradient at the interface. The time scale of the LSSE must be influenced additionally by a second, rather slower process. On the basis of this argument, the first term of Eq. (1) can be considered as static over the time scale of our interest ($>$20 ns). Using the phonon thermal gradient data, obtained from the COMSOL simulations, we calculated the second integral term of Eq. (1) for various effective magnon propagation lengths. The integral was computed from the interface up to the thickness of the YIG film. In Fig. 5, the normalized values of the experimentally and numerically calculated V_{LSSE} for $L = 300$, 500, and 700 nm are plotted as a function of time. Clearly, our model replicates the experimentally observed time scales of the LSSE, and the slow increase in the signal after 1 μs. Note that the very first slow

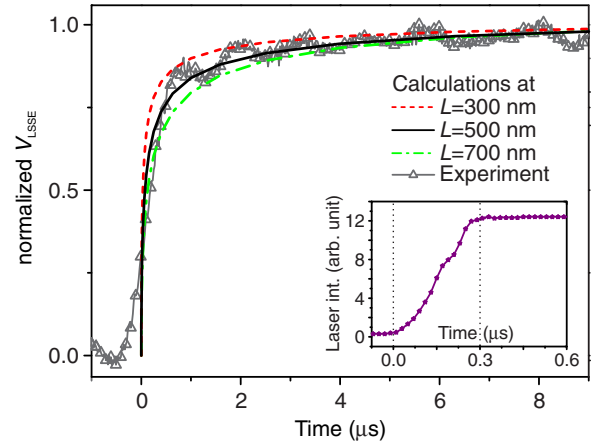FIG. 5. (Color online) Comparison of normalized values of longitudinal spin Seebeck voltage V_{LSSE}, measured experimentally, with the numerical calculations for different effective magnon diffusion lengths $L = 300$, 500, and 700 nm. The inset shows the switching time ($\approx$0.25 μs) of the laser intensity.

increase in the normalized values of V_{LSSE} (for time $\leqslant 0$ μs) originates from the switching time of the laser ($\approx$0.25 μs), shown in the inset in Fig 5. On comparing the calculated values of V_{LSSE} with the experimental results, we estimate the effective magnon diffusion length to be $\approx$500 nm. This length exhibits the depth of the YIG material over which the thermal gradient is crucial for the LSSE.

Our model reveals that the temporal evolution of the LSSE depends on the thermal gradient in the vicinity of the YIG|Pt interface. Further, thermal magnons up to a depth of a few hundreds of nanometer in YIG are effectively contributing to the LSSE. The typical effective magnon diffusion length of 500 nm agrees with recent theoretical calculations [34,35] and time-resolved SSE experiments on the ultrathin YIG films [36]. These results support the findings in Refs. [16,17] that parasitic interface effects such as the proximity Nernst effect have negligible influence on the longitudinal spin Seebeck effect in this particular system.

In conclusion, we have presented the time-resolved measurements of the longitudinal spin Seebeck effect in YIG|Pt bilayers performed by the laser heating experiments. Our findings reveal that the rise time of the LSSE is sub-microsecond fast, and the LSSE signal attains its maximum within a few microseconds, though the temperature in the system establishes in milliseconds. The time scale of the LSSE is independent of the strength of the heating source. From our model of the magnon diffusion in thermal gradients, we find that the LSSE is governed by the diffusion of the thermal magnons from the interface toward the bulk. Moreover, the establishment of the thermal gradient in the vicinity of the YIG-film interface determines the time scales of the LSSE. Our model estimates a typical diffusion length for thermal magnons to be around 500 nm in the YIG|Pt system. Our results provide an important piece of information about the time scales of the longitudinal spin Seebeck effect that shed light on the underlying physics, which might contribute to the development of future applications of spin caloritronics.

---

[1] *Spin Caloritronics*, edited by G. E. W. Bauer, A. H. MacDonald, and S. Maekawa, special issue of Solid State Commun. **150**, 459 (2010).

[2] K. Uchida, S. Takahashi, K. Harii, J. Ieda, W. Koshibae, K. Ando, S. Maekawa, and E. Saitoh, Nature (London) **455**, 778 (2008).

[3] K. Uchida, H. Adachi, T. An, T. Ota, M. Toda, B. Hillebrands, S. Maekawa, and E. Saitoh, Nat. Mater. **10**, 737 (2011).

[4] C. M. Jaworski, J. Yang, S. Mack, D. D. Awschalom, J. P. Heremans, and R. C. Myers, Nat. Mater. **9**, 898 (2010).

[5] C. M. Jaworski, J. Yang, S. Mack, D. D. Awschalom, R. C. Myers, and J. P. Heremans, Phys. Rev. Lett. **106**, 186601 (2011).

[6] K. Uchida, J. Xiao, H. Adachi, J. Ohe, S. Takahashi, J. Ieda, T. Ota, Y. Kajiwara, H. Umezawa, H. Kawai, G. E. W. Bauer, S. Maekawa, and E. Saitoh, Nat. Mater. **9**, 894 (2010).

[7] K. Uchida, H. Adachi, T. Ota, H. Nakayama, S. Maekawa, and E. Saitoh, Appl. Phys. Lett. **97**, 172505 (2010).

[8] G. E. W. Bauer, E. Saitoh, and B. J. van Wees, Nat. Mater. **11**, 391 (2012).

[9] E. Saitoh, M. Ueda, H. Miyajima, and G. Tatara, Appl. Phys. Lett. **88**, 182509 (2006).

[10] A. Kirihara, K. Uchida, Y. Kajiwara, M. Ishida, Y. Nakamura, T. Manako, E. Saitoh, and S. Yorozu, Nat. Mater. **11**, 686 (2012).

[11] J. Xiao, G. E. W. Bauer, K. C. Uchida, E. Saitoh, and S. Maekawa, Phys. Rev. B **81**, 214418 (2010).

[12] H. Adachi, J. I. Ohe, S. Takahashi, and S. Maekawa, Phys. Rev. B **83**, 094410 (2011)

[13] M. Agrawal, V. I. Vasyuchka, A. A. Serga, A. D. Karenowska, G. A. Melkov, and B. Hillebrands, Phys. Rev. Lett. **111**, 107204 (2013).

[14] S. Y. Huang, X. Fan, D. Qu, Y. P. Chen, W. G. Wang, J. Wu, T. Y. Chen, J. Q. Xiao, and C. L. Chien, Phys. Rev. Lett. **109**, 107204 (2012).

[15] S. Geprägs, S. Meyer, S. Altmannshofer, M. Opel, F. Wilhelm, A. Rogalev, R. Gross, and S. T. B. Goennenwein, Appl. Phy. Lett. **101**, 262407 (2012).

[16] T. Kikkawa, K. Uchida, Y. Shiomi, Z. Qiu, D. Hou, D. Tian, H. Nakayama, X.-F. Jin, and E. Saitoh, Phys. Rev. Lett. **110**, 067207 (2013).

[17] T. Kikkawa, K. Uchida, S. Daimon, Y. Shiomi, H. Adachi, Z. Qiu, D. Hou, X.-F. Jin, S. Maekawa, and E. Saitoh, Phys. Rev. B **88**, 214403 (2013).

[18] A. Kehlberger, R. Röser, G. Jakob, and M. Kläui, arXiv:1306.0784.

[19] M. Schreier, A. Kamra, M. Weiler, J. Xiao, G. E. W. Bauer, R. Gross, and S. T. B. Goennenwein, Phys. Rev. B **88**, 094410 (2013).

[20] M. B. Jungfleisch, V. Lauer, R. Neb, A. V. Chumak, and B. Hillebrands, Appl. Phys. Lett. **103**, 022411 (2013).

[21] M. Walter, J. Walowski, V. Zbarsky, M. Münzenberg, M. Schäfers, D. Ebke, G. Reiss, A. Thomas, P. Peretzki, M. Seibt, J. S. Moodera, M. Czerner, M. Bachmann, and C. Heiliger, Nat. Mater. **10**, 742 (2011).

[22] A. Boehnke, M. Walter, N. Roschewsky, T. Eggebrecht, V. Drewello, K. Rott, M. Münzenberg, A. Thomas, and G. Reiss, Rev. Sci. Instrum. **84**, 063905 (2013).

[23] M. Weiler, M. Althammer, F. D. Czeschka, H. Huebl, M. S. Wagner, M. Opel, I.-M. Imort, G. Reiss, A. Thomas, R. Gross, and S. T. B. Goennenwein, Phys. Rev. Lett. **108**, 106602 (2012).

[24] J. Ren, Phys. Rev. B **88**, 220406 (2013).

[25] Note that ΔT is the average temperature measured over the entire Pt strip, which might be different from the local temperature at the laser spot. However, both V_{LSSE} and ΔT (or ΔR) were measured over the entire Pt strip and are dependent on the heat dynamics. Thus the comparison of the dynamics of these two quantities is valid.

[26] COMSOL: Multiphysics with Heat Transfer Module.

[27] D. Lide, *CRC Handbook of Chemistry and Physics*, 89th ed. (Taylor & Francis, London, 2008).

[28] Q. G. Zhang, B. Y. Cao, X. Zhang, M. Fujii, and K. Takahashi, J. Phys.: Condens. Matter **18**, 7937 (2006).

[29] A. M. Hofmeister, Phys. Chem. Miner. **33**, 45 (2006).

[30] A. E. Clark and R. E. Stranka, J. Appl. Phys. **32**, 1172 (1961).

[31] M. Guillot, F. Tchéou, A. Marchand, P. Feldmann, and R. Lagnier, Z. Phys. B **44**, 53 (1981).

[32] U. Ritzmann, D. Hinzke, and U. Nowak, Phys. Rev. B **89**, 024409 (2014).

[33] S. M. Rezende, R. L. Rodríguez-Suárez, R. O. Cunha, A. R. Rodrigues, F. L. A. Machado, G. A. Fonseca Guerra, J. C. Lopez Ortiz, and A. Azevedo, Phys. Rev. B **89**, 014416 (2014).

[34] A. A. Kovalev and Y. Tserkovnyak, Europhys. Lett. **97**, 67002 (2012).

[35] S. Hoffman, K. Sato, and Y. Tserkovnyak, Phys. Rev. B **88**, 064408 (2013).

[36] N. Roschewsky, M. Schreier, A. Kamra, F. Schade, K. Ganzhorn, S. Meyer, H. Huebl, S. Geprägs, R. Gross, and S. T. B. Goennenwein, Appl. Phys. Lett. **104**, 202410 (2014).